ChemComm

Accepted Manuscript

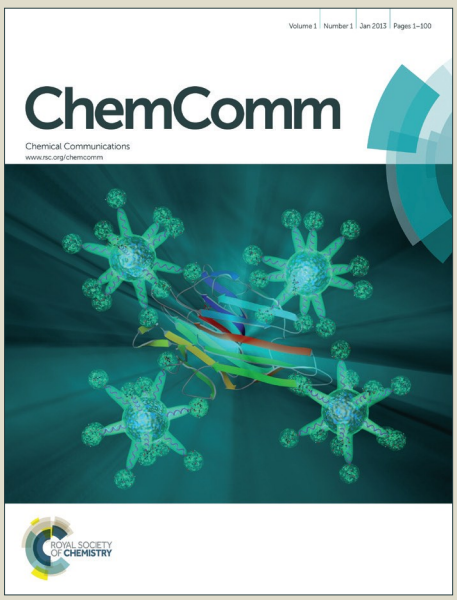

ROYAL SOCIETY OF CHEMISTRY

www.rsc.org/chemcomm

Journal Name

RSCPublishing

COMMUNICATION

Water-Soluble Plasmonic Nanosensors with Synthetic Receptors for Label-Free Detection of Folic Acid

Cite this: DOI: 10.1039/x0xx00000x

Received 00th January 2012,
Accepted 00th January 2012

DOI: 10.1039/x0xx00000x

www.rsc.org/

Randa Ahmad [a], Nordin Félidj [a], Leïla Boubekeur-Lecaque[a], Stéphanie Lau-Truong [a], Sarra Gam-Derouich [a], Philippe Decorse [a], Aazdine Lamouri [a] and Claire Mangeney*[a]

We describe an original approach to graft molecularly imprinted polymers around gold nanorods by combining the diazonium salt chemistry and the iniferter method. This chemical strategy enables a fine control of the imprinting process at the nanometer scale and provides water-soluble plasmonic nanosensors.

Gold nanorods (AuNRs) have stimulated a broad interest these past years due to their strong anisotropic optical properties which offer promising technological potential. [1-2] Indeed, AuNRs exhibit intense optical absorption peaks arising from localized surface plasmon (LSP) resonances along their long and short axes. Excitation of LSP by an external electromagnetic field results in a strong increase in the magnitude of the local electromagnetic field in the vicinity of gold nanorods, by several orders of magnitude, which is widely used for surface enhanced Raman spectroscopy (SERS). [3-4] Recently, some attempts have been made to couple gold nanoparticles (AuNPs) with molecular imprinted polymers (MIPs) for the elaboration of plasmonic-based AuNP@MIP sensors. [5-11] Molecular imprinting involves the polymerization of functional monomers in the presence of a desired template (the target analyte). The resulting polymer presents a complementary conformation to the template and provides chemical interaction with its functional groups. Subsequent removal of the imprint molecules leaves behind 'memory sites', or imprints, [12-13] and enables the polymer to rebind selectively the imprint molecule from a mixture of closely related compounds. Therefore, in AuNP@MIP sensors, a target analyte can be captured from a complex medium with a high specificity and selectivity owing to the exceptional chemical properties of the MIP matrix while the recognition event can be transduced into a physical signal (optical, electric, piezoelectric) and amplified thanks to the outstanding physical properties of the AuNPs. The large majority of plasmonic sensors based on AuNP@MIP are made of isotropic spherical NPs, which optical properties are less tunable and sensitive than anisotropic ones. The only example reported so far of gold nanorods coupled to MIPs consists in aggregated nanorods first deposited on a glass plate and then grafted with MIPs by organo-siloxane copolymerization. [14] The AuNR@MIP-coated glass substrates obtained by this approach were found efficient for the direct optical detection of protein capture and release. However, this strategy could not provide individually dispersed AuNR@MIP nanohybrids in colloidal solution, which limits its scope of application. Controlling the synthesis process in order to obtain non-aggregated colloidal AuNR@MIP is the next critical stage, which should offer several advantages such as: (i) an increase in specific surface area, the particle being in full contact with the solution containing the target molecule and (ii) their possible use for *in-situ* environmental analysis or *in-vivo* biomedical applications. The difficulty to elaborate well-controlled and non-aggregated colloidal AuNR@MIP lies on both (i) the complex surface chemistry of AuNRs, usually synthesized by the well-known seed-mediated growth approach, [15] and on (ii) their weak colloidal stability, the particles being strongly prone to aggregation. Therefore, the development of efficient chemical methods for grafting MIP layers of controlled thickness around gold nanorods dispersed and stable in aqueous medium is eminently challenging. We address this issue in the present paper by proposing an original strategy for the grafting of MIP layers on individually dispersed AuNRs, based on a combination

[a] Univ Paris Diderot, Sorbonne Paris Cite, ITODYS, UMR 7086 CNRS, 15 rue J-A de Baïf, 75205 Paris, Cedex 13, France.

Electronic Supplementary Information (ESI) available: [Synthesis, functionnalization of AuNRs, TEM images, UV-visible spectra, XPS spectra, SERS spectra and DFT modelling]. See DOI: 10.1039/c000000x/

of the diazonium salt chemistry and the iniferter polymerization method (see Figure 1). The diazonium salts are proposed here as an alternative to alkanethiol self-assembled monolayers, in order to obtain strongly attached polymerization initiator layers at the surface of AuNRs. [16-21] Complete or partial aggregation can easily occur during functionalization leading to loss of desired optical properties. Therefore, the key challenges are the preservation of the colloidal stability of the AuNR aqueous dispersion after functionalization and the subsequent covering of individual nanorods by layers of MIP with controlled thickness.

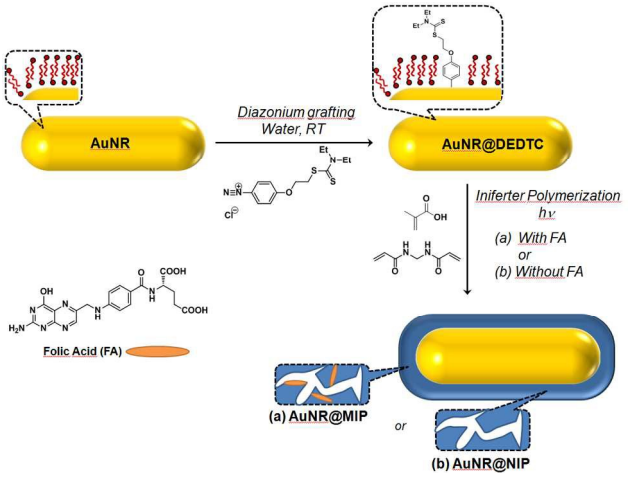

Fig. 1 Schematic illustration of the surface modification strategy for coating AuNRs with a MIP layer, by combining the diazonium salt chemistry and the iniferter photopolymerization method. AuNRs were also coated with non-imprinted polymers (NIP) as a reference sample. These hybrids are called here AuNR@NIP.

Our strategy relies on a bifunctional initiator, 2-(phenoxy)ethyldiethylcarbamadithionate diazonium chloride (Cl^-,$^+N_2$–C_6H_4–O-CH_2-CH_2–DEDTC)[22] containing (i) a diazonium end group for surface anchoring and (ii) a N,N-diethyldithiocarbamate (DEDTC) function able to activate surface-initiated photoiniferter-mediated polymerization (SI-PIMP). [23] We demonstrate this approach by grafting cross-linked molecularly imprinted co-polymers of methacrylic acid (MAA) and N,N'-methylenebisacrylamide (MBAm) on gold nanorods, in the presence of folic acid (FA), as the template molecule. Folic acid was chosen as it is a widely used water-soluble vitamin which is a significant component for human health. It relates to a series of diseases such as mental devolution, heart attack and congenital malformation. Therefore, the selective and sensitive determination of FA is important from the clinical and health viewpoints. Various methods have been developed for the determination of FA, including liquid chromatography coupled to mass spectrometry (LCMS) and high-performance liquid chromatography (HPLC). [24] However, these methods are expensive and time-consuming. Hence, the elaboration of simple and sensitive nanosensors for the detection of FA still remains challenging.

AuNRs were prepared through the well-known seed-mediated growth procedure. [15] The produced nanorods showed an average length L of 35±3 nm and a small axis d of 15±3 nm. The AuNRs were functionalized by the initiator-derived diazonium salts by simple incubation at room temperature. Then, the polymerization could proceed, mixing the AuNR@DEDTC particles with MAA as the monomer, MBAm as the crosslinking agent and FA as the template molecule. The deoxygenated mixture was irradiated under UV light for varying times (4, 6 and 8 h) to control the polymer coating thickness. The final products (AuNR@MIP_{xh}, where x stands for the polymerization time) consist of nanorods coated by molecularly imprinted polymers. A reference non-imprinted polymer sample (AuNR@NIP) was prepared using the same procedure, but without addition of the FA template.

The TEM images of the bare and functionalized AuNRs, are displayed in Figure 2. After polymerization, the gold nanorods appear to be fully coated with a uniform polymer layer, not detected on the bare AuNRs. The particles remain perfectly dispersed, evidencing the steric stabilization provided by the polymer overlayer (see Figure S1 for complementary TEM images). Interestingly, the thickness of the MIP coating can vary from ~5 nm to ~20 nm by adjusting the polymerization time (4h and 8h respectively), in agreement with the controlled character of the polymerization process.

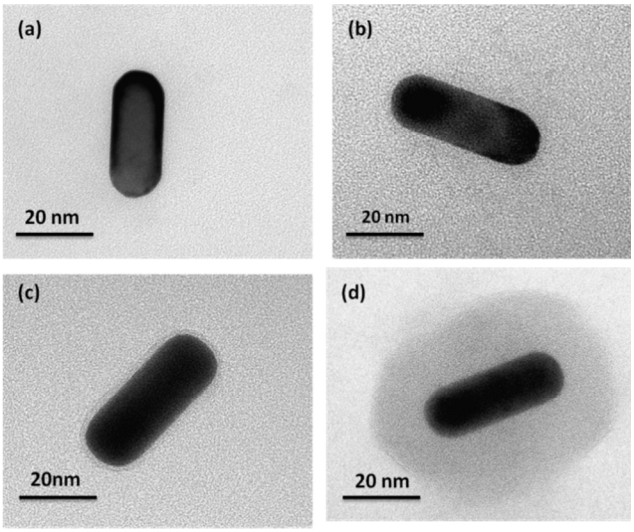

Fig. 2 TEM micrographs of gold nanorods (a) CTAB-coated AuNRs; (b) AuNR@DEDTC; (c) AuNR@MIP_{4h} after 4h polymerization and (d) AuNR@MIP_{8h} after 8h polymerization.

The UV-visible spectra of AuNRs (Figure S2) confirm that the colloidal stability of the AuNRs is preserved through the whole functionalization procedure, without any spectral broadening of the plasmon bands. The only detectable change is a red-shift (up till 56 nm) of the plasmon bands due to the coating of the AuNRs by organic layers of increasing thickness and density. The surface chemical composition of the nanohybrids was investigated by XPS. Both the survey scans and the high resolution spectra (Figure S3) reveal strong modifications after functionalization, which are summarized in Table 1. The reaction with the diazonium salt-derived initiator introduces new peaks due to the DEDTC end-groups (S2p and N1s, see high resolution spectra in Figure S4).

Table 1 Surface chemical composition (At %) of initial AuNRs, AuNR@DEDTC and AuNR@MIPs$_{xh}$ after various time of polymerization.

Material[a]	Au	C	N$^+$	N N-C	Br	S
Bare AuNRs	14.6	76.8	4.3	-	4.3	-
AuNR@DEDTC	30.9	61.3	2.3	0.5	3.4	2.1
AuNR@MIP$_{4h}$	4.5	81.0	0.5	13.0	0.8	0.7
AuNR@MIP$_{6h}$	3.0	82.3	0.5	13.5	0.7	0.5
AuNR@MIP$_{8h}$	ε	86.2	0.5	13.1	0.3	0.4

Concomitantly, the signals due to the CTAB bilayer (Br3d and N$^+$) decrease, indicating the partial exchange of CTAB by the initiator molecules at the surface of AuNRs. No peak that would be attributed to nitrogen atoms from the diazonium group can be observed, evidencing the complete transformation of the diazonium cations. After polymerization, the most striking observation is the progressive decrease of the gold signal (Au4f at 84.3 eV) and the relative increase of carbon and nitrogen due to the poly(MAA-co-MBAm) coating. Interestingly, while the Au surface is almost completely screened by the polymer chains, the S2p signal is still detectable after 8 hours of polymerization, confirming the living character of the polymerization process, leaving the DEDTC moieties at the chain extremities.

The Au@DEDTC samples were further characterized by surface enhanced Raman scattering (SERS). The comparison of the normal Raman spectrum of DEDTC-diazonium salt (see Fig. S5) with the SERS spectra after grafting on AuNRs, shows the disappearance of the strong band at 2246 cm^{-1} corresponding to the N≡N stretching vibration. Upon increasing the diazonium concentration, the strong band at 178 cm^{-1} (red arrow, Figure 3a) commonly assigned to the Au-Br bond stretching (adsorption of CTAB on gold surface) decreases. Concomitantly, a close band at 207 cm^{-1} appears on the spectra. Characteristic bands expected around 270 cm^{-1} and 1800 cm^{-1} for the S-Au and N=N (in Au-N=N) stretching modes could not be observed on the SERS spectra. [25-26] Besides, HR-XPS signal for S2p, is located at 164.0 eV, which is 2eV higher than the expected binding energy for S coordinated to Au. [27] Therefore, the grafting on gold through sulfur (resulting from cleavage of DEDTC moiety) or through nitrogen (direct attachment of diazonium group via the cationic mechanism) can be ruled out. In an attempt to assign the main bands and to locate the Au-C stretching vibration on SERS spectra, DFT calculations were conducted on the model system methoxyphenyl bonded to gold cluster Au$_{20}$. Two binding configurations were considered to mimic the coordination of the aryl group on the AuNRs: in the first one, the Au-C bond involves the vertex of the pyramidal Au$_{20}$ cluster corresponding to an ad-atom site (MeOPh-Au$_{20}$v) while in the second one, the Au-C bond involves one face of the cluster corresponding to the (111) fcc gold face (MeOPh-Au$_{20}$f). For the sake of clarity and since the band positions are similar for both configurations, the DFT simulated spectra will only be discussed for the on face model. In addition to the monolayer model on gold surface, the grafting of multilayers of aryl groups was also considered using biphenyl adducts on gold (see Figure S6).

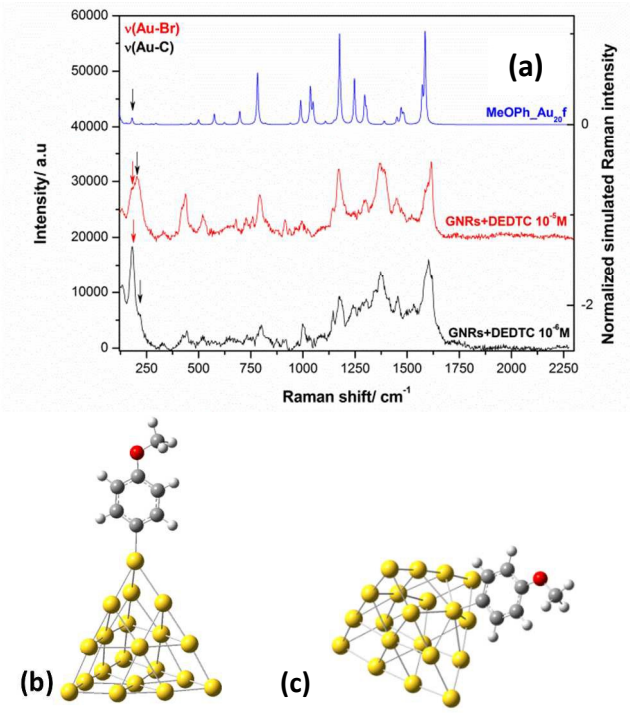

Fig. 3 (a) Experimental SERS spectra (λ_{exc}= 633 nm) of AuNR@DEDTC (incubated with 10^{-6}M (black) or 10^{-5}M (red) of diazoDEDTC) and simulated Raman spectrum for the model MeOPh-Au$_{20}$f (blue). Black and red arrows locate respectively Au-C and Au-Br stretching modes. DFT-Optimized structures of the model system MeOPh **(b)** on the vertex and **(c)** on the face of the pyramidal Au$_{20}$ cluster.

Except for bands at 436, 522 and 1372 cm^{-1}, the simulated Raman spectra for MeOPh-Au$_{20}$ model system are in good agreement with the experimental SERS. The Au-C stretching vibration is predicted by DFT at 185 cm^{-1} for MeOPh-Au$_{20}$f which could be correlated with the observed band at 207 cm^{-1} on the SERS spectra. It is worth mentioning that the Au-C stretching mode appears for DEDTC derivative at significantly lower Raman shift as compared to the electron withdrawing p-nitrophenyl modified gold surface studied elsewhere. [18, 21] The remaining bands not predicted by simulation on the simple model used here are very characteristic vibrational signatures of diethyldithiocarbamate group at 436 (δ(CH$_2$NCH$_2$)), 522 (δ(CH$_2$NC)) and 1372 cm^{-1} (δ(NCH) and ν(C-N)). [28] These observations point to the spontaneous reduction of the diazonium cation to the corresponding phenyl radical leading likely to the formation of Au-C bond.

SERS was then used to study the capture and release of FA from AuNR@MIP. Figure 4 compares the Raman bands of free FA and the SERS bands of FA in the AuNR@MIP hybrid before and after extraction of the template. The strongest SERS peaks characteristic of FA, located at 1595 cm^{-1} and 1365 cm^{-1} were chosen as the signature to account for the concentration of folic acid in the samples[29]. These bands are clearly visible in the spectrum of AuNR@MIP after their synthesis evidencing the presence of the FA template within the MIP shell. In contrast, these bands disappear almost completely after acetic acid treatment, confirming the efficient extraction of the FA template from the hybrid particles. The binding properties of AuNR@MIP

towards FA were then determined by measuring the uptake of FA in water over a range of concentrations from 10^{-8} to 10^{-4} mol.L^{-1}. The intensities of the SERS bands due to FA increase progressively with rising concentration of FA (Figure S7), indicating the efficient uptake of FA by the nanohybrids.

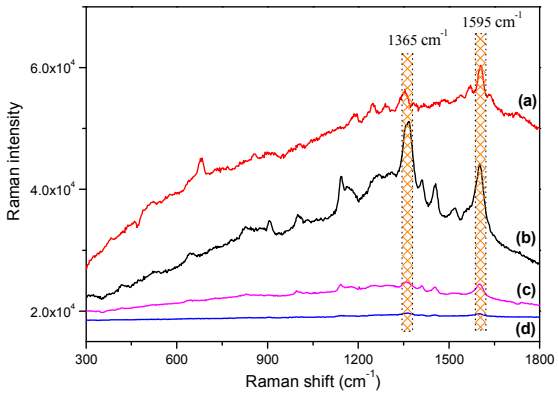

Fig. 4 a) Raman spectrum of free FA; b) SERS of FA on AuNR@MIP after synthesis, c) SERS of FA at 0.1 μM, extracted by AuNR@MIP and d) SERS spectrum obtained after complete extraction of FA from AuNR@MIP.

The binding amount of FA was found five times higher for AuNR@MIP than AuNR@NIP evidencing the strong specificity of the nanohybrids. A high selectivity was also demonstrated using folinic acid as a structurally related molecule (see Figure S8), confirming the presence of specific rebinding sites in the polymer overlayer of the MIP particles offering a steric and an electronic microenvironment complementary to that of FA. The minimum concentration of folic acid detected was around 0.1 μM which is lower than the calculated limit of detection reported by R. C. Advincula (15.4 μM) using an electropolymerized molecularly imprinted polymer film on a quartz crystal microbalance, [30] indicating that sensitive detection of FA was achieved here, based on colloidal AuNR@MIP.

Conclusions

In summary, we have developed an original and simple route combining the aryl diazonium salt chemistry and the iniferter method to elaborate individually dispersed hybrid materials composed of gold nanorod cores and molecular imprinted polymer shells. The plasmonic properties of the nanorods enable the direct detection of FA capture and release. Our approach offers several advantages over conventional methods: (i) ease and rapidity of gold nanorods surface functionalization using diazonium salts; (ii) presence of a covalent binding between the inorganic core and the organic coating; (iii) formation of individually dispersed AuNR@MIP. We do believe this synthetic approach will provide a new general nanomaterial strategy design for the grafting of MIPs on AuNRs.

Notes and references

1. H. Chen, L. Shao, Q. Li and J. Wang, *Chem. Soc. Rev*, 2013, **42**, 2679-2724.
2. S. N. X. Huang, M. A. El-Sayed, , *Adv. Mater.*, 2009, **21**, 4880.
3. N. Felidj, J. Aubard, G. Levi, J. R. Krenn, M. Salerno, G. Schider, B. Lamprecht, A. Leitner and F. R. Aussenegg, *Phys. Rev. B* 2002, **65**, 075419/075411-075419/075419.
4. S. Kessentini, D. Barchiesi, C. D'Andrea, A. Toma, N. Guillot, E. Di Fabrizio, B. Fazio, O. M. Marago, P. G. Gucciardi and M. L. de la Chapelle, *J. Phys. Chem. C*, 2014, **118**, 3209-3219.
5. A. A. Volkert and A. J. Haes, *The Analyst*, 2014, **139**, 21-31.
6. M. Riskin, R. Tel-Vered, M. Frasconi, N. Yavo and I. Willner, *Chem.-Eur. J.*, 2010, **16**, 7114-7120.
7. J. Matsui, K. Akamatsu, S. Nishiguchi, D. Miyoshi, H. Nawafune, K. Tamaki and N. Sugimoto, *Anal. Chem.*, 2004, **76**, 1310-1315.
8. A. Gultekin, A. Ersoz, D. Hur, N. Y. Sariozlu, A. Denizli and R. Say, *Sens. Actuators, B*, 2012, **162**, 153-158.
9. S. Gam-Derouich, S. Mahouche-Chergui, S. Truong, D. Ben Hassen-Chehimi and M. M. Chehimi, *Polymer*, 2011, **52**, 4463-4470.
10. M. L. Yola, T. Eren and N. Atar, *Sens. Actuators, B*, 2015, **210**, 149–157.
11. M. L. Yola, T. Eren and N. Atar, *Biosens. Bioelectron.*, 2014, **60**, 277-285.
12. L. Ye and K. Mosbach, *Chem. Mater*, 2008, **20**, 859-868.
13. Y. Fuchs, O. Soppera and K. Haupt, *Anal. Chim. Acta*, 2012, **717**, 7-20.
14. A. Abbas, L. M. Tian, J. J. Morrissey, E. D. Kharasch and S. Singamaneni, *Adv. Funct. Mater.*, 2013, **23**, 1789-1797.
15. B. Nikoobakht and M. A. El-Sayed, *Chem. Mater*, 2003, **15**, 1957-1962.
16. J. Pinson and F. Podvorica, *Chem. Soc. Rev.*, 2005, **34**, 429-439.
17. F. Mirkhalaf, J. Paprotny and D. J. Schiffrin, *J. Am. Chem. Soc.*, 2006, **128**, 7400-7401.
18. L. Laurentius, S. R. Stoyanov, S. Gusarov, A. Kovalenko, R. B. Du, G. P. Lopinski and M. T. McDermott, *ACS Nano*, 2011, **5**, 4219-4227.
19. Y. Aït Atmane, L. Sicard, A. Lamouri, J. Pinson, M. Sicard, C. Masson, S. Nowak, P. Decorse, J.-Y. Piquemal, A. Galtayries and C. Mangeney, *J. Phys. Chem. C.*, 2013, **117**, 26000-26006.
20. N. Griffete, R. Ahmad, H. Benmehdi, A. Lamouri, P. Decorse and C. Mangeney, *Colloids Surf. A: Physicochem. Eng. Asp.*, 2013, **439**, 145-150.
21. R. Ahmad, L. Boubekeur-Lecaque, M. Nguyen, S. Lau-Truong, A. Lamouri, P. Decorse, A. Galtayries, J. Pinson, N. Felidj and C. Mangeney, *J. Phy. Chem, C*, 2014, **118**, 19098-19105.
22. R. Ahmad, N. Griffete, A. Lamouri and C. Mangeney, *J. Colloid Interface Sci.*, 2013, **407**, 210-214.
23. T. Otsu, *J. Polym. Sci., Part A: Polym. Chem.*, 2000, **38**, 2121-2136.
24. J. Arcot and A. Shrestha, *Trends Food Sci. Technol.*, 2005, **16**, 253-266.
25. S. Sanchez-Cortes, C. Domingo, J. V. Garcia-Ramos and J. A. Aznarez, *Langmuir*, 2001, **17**, 1157-1162.
26. B. Varnholt, P. Oulevey, S. Luber, C. Kumara, A. Dass and T. Buergi, *J. Phys. Chem. C*, 2014, **118**, 9604-9611.
27. Y. Zhao, W. Perez-Segarra, Q. C. Shi and A. Wei, *J. Am. Chem. Soc.*, 2005, **127**, 7328-7329.
28. R. Mattes, L. Zhengyan, M. Thunemann and H. Schnockel, *J. Mol. Struct.*, 1983, **99**, 119-132.
29. W. Ren, Y. Fang and E. Wang, *ACS Nano*, 2011, **5**, 6425-6433.
30. D. C. Apodaca, R. B. Pernites, R. R. Ponnapati, F. R. Del Mundo and R. C. Advincula, *ACS Appl. Mater. Interfaces*, 2011, **3**, 191-203.